Available online at www.sciencedirect.com
SCIENCE DIRECT®
PERGAMON
International Journal of Heat and Mass Transfer 46 (2003) 3967–3974
International Journal of HEAT and MASS TRANSFER
www.elsevier.com/locate/ijhmt

Examination of ratiometric laser induced fluorescence thermometry for microscale spatial measurement resolution

H.J. Kim [a], K.D. Kihm [b,*], J.S. Allen [c]

[a] Division of Mechanical and Industrial Engineering, Ajou University, Suwon 442-749, South Korea
[b] Department of Mechanical Engineering, Texas A&M University, College Station, TX 77843-3123, USA
[c] The National Center for Microgravity Research, NASA Glenn Research Center, Cleveland, OH 44135, USA

Received 22 November 2002; received in revised form 2 May 2003

Abstract

Ratiometric laser induced fluorescence (LIF) thermometry technique has been quantitatively examined for its capability for a microscale field-of-view. The goal of the study is to quantitatively examine the measurement accuracy of the ratiometric LIF technique at sub-millimeter and micron scales for its potential use as a microscale temperature mapping tool. Measurements have been made for the steady temperature fields established by thermal buoyancy inside 1-mm wide closed test cell with low Grashof–Prandtl numbers ($86 < Gr_wPr < 301$), and the detailed measured data have been compared with the well-known predictions. The smallest measurement resolution could be achieved being equivalent to the CCD pixel size of 4.7 μm in the present experiment, but with large data uncertainties. The measurement uncertainties show persistent improvement to better than ±1 °C when measurement resolution is equivalent to 76 μm.

1. Introduction

Among the available means of temperature measurement probes, there is no question regarding the extensiveness and rigorousness of thermocouple (TC) probes for a wide range of heat transfer applications. A carefully calibrated TC probe is capable of measuring temperatures with better than ±0.1 K precision [1]. Two primary limitations of TC probes, however, are their relatively large spatial resolution, on the order of a few hundred microns in the conventional sense, and their physical intrusiveness in the flow. These limitations diminish the possibility of using TC probes for microscale heat transfer applications. In addition, their point measurement nature makes full-field temperature mapping very cumbersome as a large number of probes must be placed and monitored simultaneously.

Thermochromic liquid crystal (TLC) probes [2,3] are based on the temperature dependence of their optical properties in a predictable and repeatable manner. When TLC is illuminated, TLC selectively reflects light at a visible wavelength characterized by the local temperature. This relationship of color to temperature has allowed researchers to quantitatively map temperature distribution [4,5]. A difficulty in using TLC is that one has to calibrate each point of test field to compensate for the influence of the illuminating light variation [6]. The color bias occurring from the wall reflection and scattering is another obstacle in applying the TLC technique to full-field mapping. The relatively larger sizes of microencapsulated TLC beads, typically on the order of 10 μm or larger, are considered too large for microscale measurement resolution.

The laser induced fluorescence (LIF) technique [7,8] uses fluorescence dye molecules as seeding particles and the use of temperature sensitive fluorescent dyes showed LIF as a feasible temperature mapping technique [9–11]. The fluorescence intensity is proportional to the illuminating light intensity, dye concentration and optical

* Corresponding author. Tel.: +1-979-845-2143; fax: +1-979-862-2418.
E-mail address: ken-kihm@tamu.edu (K.D. Kihm).

0017-9310/03/$ - see front matter © 2003 Elsevier Ltd. All rights reserved.
doi:10.1016/S0017-9310(03)00243-6

constant of the dye called quantum efficiency [12]. Therefore, if the illumination light is perfectly uniform and the dye concentration remains constant, the fluorescence intensity may be considered, in principle, to depend only on temperature. However, in practice, it is very difficult to ensure a homogeneous incident light intensity distribution, if not impossible, since the laser sheet intensity progressively decreases due to the absorption/scattering by dye molecules as it progresses in the test medium even under an ideal optical configuration. Furthermore, the optical limitation and uncertainty of the CCD camera response can hardly guarantee persistent intensity levels from test to test.

One way to correct for the spatial nonuniformity would be to carry out point-by-point corrections for measured LIF images using a large set of reference images taken at several different temperatures, so that the dependency of LIF quenching can be appropriately accounted for, the local temperature as well as for the spatial nonuniformities of the background illumination. However, this requires that the imaging field configurations be precisely identical for both calibration and measurement, which in turn requires the use of the same setup for both calibration and measurement. This makes the LIF technique using a single dye very cumbersome in that a new calibration will be needed for every different experimental configuration.

A more reliable and noble way to bypass these issues is to normalize the fluorescence intensity of the temperature dependence dye with a temperature independent dye. This ratiometric LIF, as it has come to be known originated from the field of biology, is also called dual emission LIF [13] and two-color LIF [14,15]. Coppeta and Rogers [13] comprehensively describes the technique and showed experimental results to demonstrate the feasibility, for not only temperature but also pH as well, for the case of a moderate scale test field of 100-mm thermal plume. Sakakibara and Adrian [14,15], which came out about the same time, showed a calibration uncertainties of ±1.5 K over a 25 K temperature range and applied this technique to measure a three-dimensional thermal convection field above a heated horizontal surface of 40-mm square in dimension.

The present work uses a similar ratiometric LIF technique to quantitatively examine the measurement accuracy, in conjunction with its spatial resolution, for feasibility as a microscale temperature field-mapping tool. A 1.0-mm wide cuvette is heated differentially on opposite vertical sides so as to generate a natural convection thermal field, with relatively low Grashof–Prandtl number, $Gr_wPr < 300$, and the resulting steady temperature field has been measured by the ratiometric LIF technique. The measurement accuracy is assessed by comparing the measured temperature field with computational predictions, which can be considered accurate for the near-conduction regime of low Gr_wPr, and the measurement uncertainties are determined for different spatial resolutions ranging from 4.2 to 76 μm.

2. Experimental setup

The present system uses Rhodamine-B (absorption peak at 554 nm and emission peak at 575 nm) as a temperature sensitive dye, as high as 2% intensity change per K, and Rhodamine-110 (absorption peak at 496 nm and emission peak at 520 nm) as a temperature insensitive dye, as low as 0.13%/K. Both fluorescent dyes are pumped by the "blue" Ar-ion CW laser light band-peaked at 488 nm.

In the absence of the pH-dependence of both dyes, the intensity ratio of the two fluorescence emissions is given as

$$\frac{I_{\mathrm{rhb}}}{I_{\mathrm{rh110}}} = \frac{I_{0\mathrm{rhb}}\varepsilon_{\mathrm{rhb}}[c]_{\mathrm{rhb}}Q_{\mathrm{rhb}}}{I_{0\mathrm{rh110}}\varepsilon_{\mathrm{rh110}}[c]_{\mathrm{rh110}}Q_{\mathrm{rh110}}} \tag{1}$$

where the ratio of the absorption spectral intensity, $I_{0\mathrm{rhb}}/I_{0\mathrm{rh110}}$, is invariant when a single illumination source is used for both dyes, and the molar absorptivity ε is nearly independent of temperature [12]. For a fixed concentration ratio of the two dyes, $[c]_{\mathrm{rhb}}/[c]_{\mathrm{rh110}}$, the fluorescence intensity ratio, $I_{\mathrm{rhb}}/I_{\mathrm{rh110}}$, will only depend on the quantum efficiency ratio, $Q_{\mathrm{rhb}}/Q_{\mathrm{rh110}}$, which may be correlated to temperature. A careful calibration is needed to determine a functional correlation between the fluorescent intensity ratio ($I_{\mathrm{rhb}}/I_{\mathrm{rh110}}$) and temperature of test medium containing small concentrations of both fluorescent dyes.

The use of two-cameras [14,15], with a dichroic beam splitter, can simultaneously detect both emissions from the two fluorescent dyes. However, the pixel-by-pixel correspondence between the two camera images must be ensured by a reference-imaging object such as a grid plate [16]. Furthermore, the use of the beam splitter will alter the spectral characteristics of the transmitted and reflected wavelengths because of the wavelength-dependent dispersion of the inclined incoming rays at 45° incident angle onto the beam splitter [17]. Thus, the intensity ratio at a given temperature becomes spatially dependent within the image plane, and this requires a cumbersome point-by-point calibration for the entire field-of-view over a range of temperatures.

The single-camera system (Fig. 1) sequentially detects each fluorescence signal by alternating the two band-pass filters, a long-pass filter ($\lambda_T > 560$ nm) for Rh-B detection and a narrow band-pass filter (505 nm $< \lambda_T <$ 515 nm) for Rh-110 detection. Since the camera detects para-normal incident rays the spectral dispersion problem is minimized and the need for point-by-point calibration is not necessary. Also, the single-camera system requires less attention to image coincidence and is relatively insensitive to external vibrations. The primary

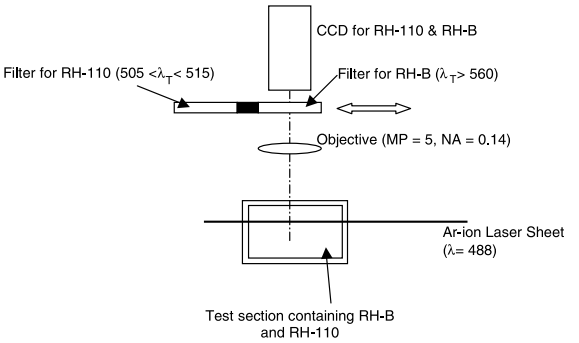

Fig. 1. Schematic illustration of the modified ratiometric LIF thermometry system.

limitation of the simplified system is resulted from the sequential image recording, and the single-camera system is unable to handle unsteady thermal problems. The single-camera ratiometric LIF system, however, is believed to be more reliable and convenient than the dual camera setup for investigating steady thermal problems.

3. Calibration experiments

A calibration experiment was conducted using an isothermal cuvette immersed in a constant temperature chamber in order to determine the correlation between the fluorescence intensity ratio and temperature. The 15-cm cubic constant temperature chamber is made of 6.3-mm thick insulated plexiglass and the chamber is connected to a thermobath to complete a closed loop circulation of constant temperature fluid (water). The calibration cuvette of 10-mm square cross-section and 50-mm long was filled with purified water containing 6-mg/l concentration of Rh-B and 1-mg/l concentration of Rh-110. The cuvette was placed within the constant temperature chamber and chamber temperature was monitored using a K-type thermocouple probe. It took approximately 20 min until temperature of thermocouple reached to set temperature within ±0.5 °C. Fluorescence was induced using a laser sheet passing through the top of the cuvette and the fluorescence intensity signals were detected through a 3.5-cm square optical window located in the front wall of the constant temperature chamber.

An interline transfer monochromatic CCD camera (maximum 640×480 pixels resolution, approximately 9.0 μm pixel size, Sony XC-73) with a Mitutoyo 5× objective lens (NA = 0.14) having an extended working distance of approximately 37 mm was used to record images of an approximately 3.0 mm × 2.0 mm. Note that due to the chemical and photochemical decomposition, the emission intensity of fluorescence dye degrades during repeated excitation and emission transitions [18]. The lowered fluorescence emission levels of degraded dyes made LIF images difficult to record. What we have found for the best to achieve accuracy and repeatability is to use fresh mixtures not older than two or three days.

Fig. 2 plots fluorescence intensity for the two dyes (Rh-B and Rh-110) against a temperature range of 16–40 °C, where different symbols represent individual data sets taken at three different times during the calibration period ensuring the acceptable repeatability. Each data point represents the average intensity of the central 1.5-mm × 1.0-mm field-of-view (320 by 240 pixels), in order to exclude the potentially degraded image of the off-axis region, and averaged for ten (10) recorded images. The discrepancy between the three calibration data sets are less than 5%. Though the entire calibration test section should remain ideally at a uniform temperature, the aforementioned nonideal optical and thermal factors may result in slight spatial nonuniformity in the fluorescence intensity. These nonideal factors include nonuniformity in the background illumination, which cannot be completely abated, inherent fluorescence intensity variations due to thermal drift of dye molecules caused by small temperature gradients in the cuvette, and by imperfections and unsteady noise in the CCD pixels.

Assuming a normal distribution of the measured temperature data scattered around the expected value (m), the calibration uncertainty levels are estimated based on a 95%-confidence level standard deviation ($\pm 2\sigma$). Table 1 shows the calibration uncertainties depending on the interrogation cell sizes, with the maximum uncertainty shown for the pixel-by-pixel variation (4.7-μm by 4.2-μm spatial resolution) and zero uncertainty when averaged for the whole calibration field-of-view (1.5-mm by 1.0-mm spatial resolution). Each uncertainty value represents the average across the tested

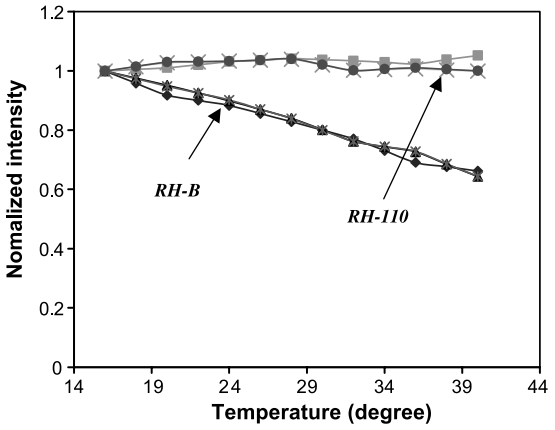

Fig. 2. Comparison of fluorescence intensities of RH-B and RH-110, normalized by the corresponding intensities at 14 °C, for calibration data for the two-color ratiometric thermometry.

Table 1
Dependence of the calibration uncertainties with 95% confidence level on the interrogating cell size

Interrogation cell (pixels)	Spatial resolution (μm)	Intensity ratio uncertainties	Temperature uncertainties (°C)
1 by 1	4.7×4.2	±0.143	±5.635
10 by 10	47×42	±0.056	±2.964
32 by 24	150×100	±0.043	±1.967
64 by 48	300×200	±0.033	±1.496
128 by 96	600×400	±0.022	±1.006
256 by 192	1200×800	±0.009	±0.412
320 by 240	1500×1000	±0	±0

temperature range from 16 to 40 °C, and ten images at each temperature. The measured temperature uncertainties exhibit an adverse dependence on the interrogating cell size, showing dramatic decrease with increasing interrogation cell size. For example, the calibration uncertainty decreases from ±1.967 °C for 150-μm by 100-μm interrogation cell to ±0.412 °C for 1200-μm by 800-μm interrogation cell.

Brownian diffusive motion may become a considerable factor when sub-micron particles are used for a tracer since the particle diffusivity rapidly increases with decreasing particle diameter. The molecular weight of Rh-B and Rh-110 are heavier than the surrogating water molecules by an order of magnitude or more [19]. Water molecule size is known to be about 0.14 nm and Rhodamine particle sizes are estimated to be an order of a few nanometers [20]. Therefore, these ''particles'' are expected to rather disperse as small particles than dissolve as molecules such as for alcohol–water mixture. In addition, the Rhodamine dyes are likely to form a large cluster due to their highly probable coagulation in water unless special care is exercised to eliminate coagulation. It is believed that the Brownian motion can describe the dispersion of Rh-B and Rh-110 ''compound'' dye molecules to an extent.

The root-mean-square (r.m.s.) particle displacement by the Brownian motion during an elapsed time interval Δt is given as $\bar{x} \approx \sqrt{2D \cdot \Delta t}$ [21], and the diffusivity is given as [22],

$$D = \frac{kT}{3\pi\mu d_{\mathrm{p}}} \approx 4.29 \times 10^{-10}\ \mathrm{m^2/s} \tag{2}$$

where $d_{\mathrm{p}} \approx 1.0$ nm for individual fluorescent compound dye molecules (in reality, coagulated dye molecules can form a cluster as large as 50 nm as evidenced by transmission electron microscopy (TEM) at Texas A&M Electron Microscopy Center), the absolute viscosity of water $\mu = 1.0 \times 10^{-3}$ N s/m^2 at 20 °C, and the Boltzmann's constant $k = 1.38 \times 10^{-23}$ J/K. For the recording period of $\Delta t = 0.05$ s (corresponding to the maximum recording time for 20 fps, and Δt can be substantially shorter when an electronic shutter controls the exposure time), the Brownina displacement is approximately 4.6 μm. In other words, the Brownian diffusion may render the spatial resolution with ±4.6-μm uncertainties.

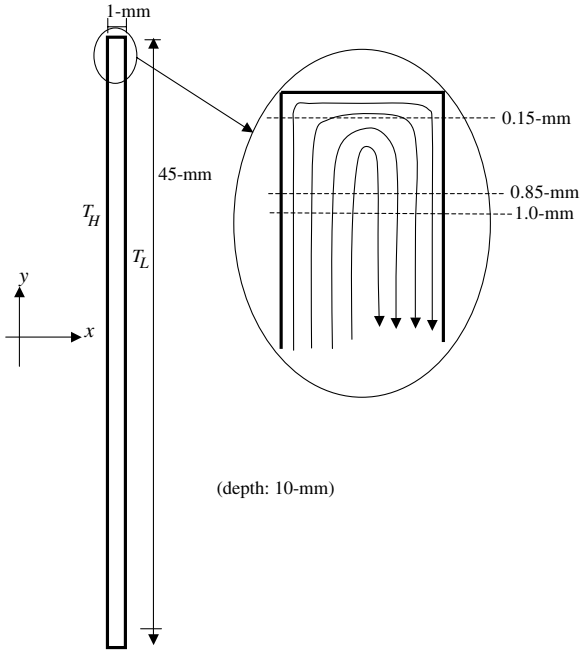

Fig. 3. Test cuvette consisting of heated (T_{H}), cooled (T_{L}), and adiabatic top and bottom walls.

4. Results and discussion

The test cuvette (Fig. 3) has dimensions of 1-mm wide (w), 10-mm deep (d), and 45-mm high (h). Each of the two sidewalls (10-mm deep and 45-mm high) is maintained at a different temperature by conduction from an attached copper jacket through which water circulates to and from a controlled thermobath. The temperature differential between the two sidewalls establishes a steady, thermally-driven buoyant flow, as schematically shown in the inset illustration of Fig. 3. The top and bottom surfaces of the cuvette are insulated to provide an adiabatic condition. A thermocouple probe embedded near the middle of each sidewall, at 0.1-mm depth from the contacting surface, monitors the surface temperature persistence.

The experimental results are compared with numerical predictions to locally and quantitatively examine the measurement accuracy and spatial resolution. The pertinent laminar natural convection flow inside a closed rectangular boundary is predicted using a standard computational technique. The conventional finite volume method [23,24] is used to solve the two-dimensional and steady-state mass, momentum and energy equations for temperature and velocity fields for the identical boundary conditions as used in the experiments. The following assumptions are made for the mathematical formulation used for modeling:

1. The working fluid is Newtonian, with a constant viscosity, and incompressible.
2. All thermophysical properties are assumed remaining constant at 300 K.
3. No-slip boundary conditions are applied to the channel wall.
4. The Boussinesq approximation for the momentum transport is used to accommodate the buoyant effect due to the thermal convection density variation.

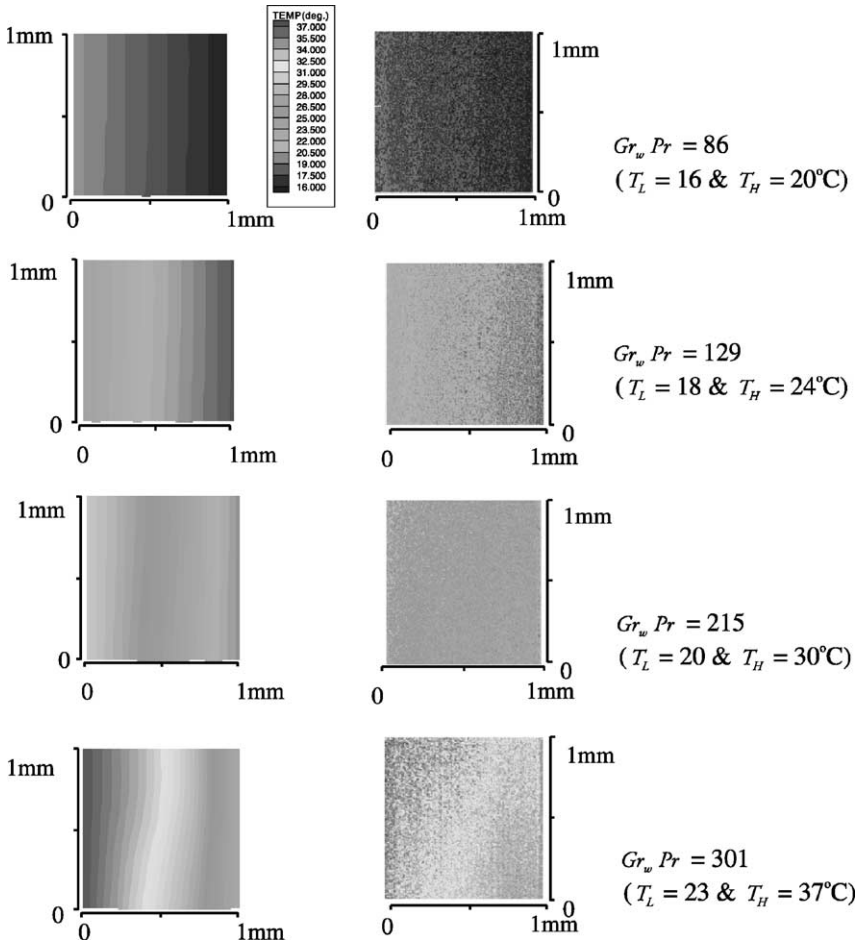

Fig. 4. Calculated (the left column) and measured (the right column) temperature contours for the top 1.0-mm by 1.0-mm region.

The dependent variables of T, p, u, and v are iteratively calculated from the elliptical momentum and energy equations. The uniform grid dimension is set to 17 across the 1-mm channel width and 540 for the 45-mm height, and thus, the computational grid size is set to approximately 58.8 μm by 83.3 μm. Although not shown, smaller grid sizes do not alter the resulting solutions.

Fig. 4 shows comparison between the calculated (the left column) and the measured (the right column) temperature distributions for the top 1.0-mm by 1.0-mm square region of the test cuevette. Four different wall temperature differentials, 16–20, 18–24, 20–30 and 23–37 °C, are considered with their corresponding Grashof–Prandtl number, $Gr_wPr \equiv \frac{g\beta\Delta Tw^3}{\nu^2}\cdot\frac{\nu}{\alpha} = 86$, 129, 215, and 301, respectively (at 300 K, the expansion coefficient, $\beta = 2.76\times10^{-4}$ K^{-1}, the kinematic viscosity of water, $\nu = 8.567\times10^{-7}$ m^2/s, the thermal diffusivity, $\alpha = 1.470\times10^{-7}$ m^2/s, and the channel width, $w = 1.0$ mm). The measured and calculated temperature contours

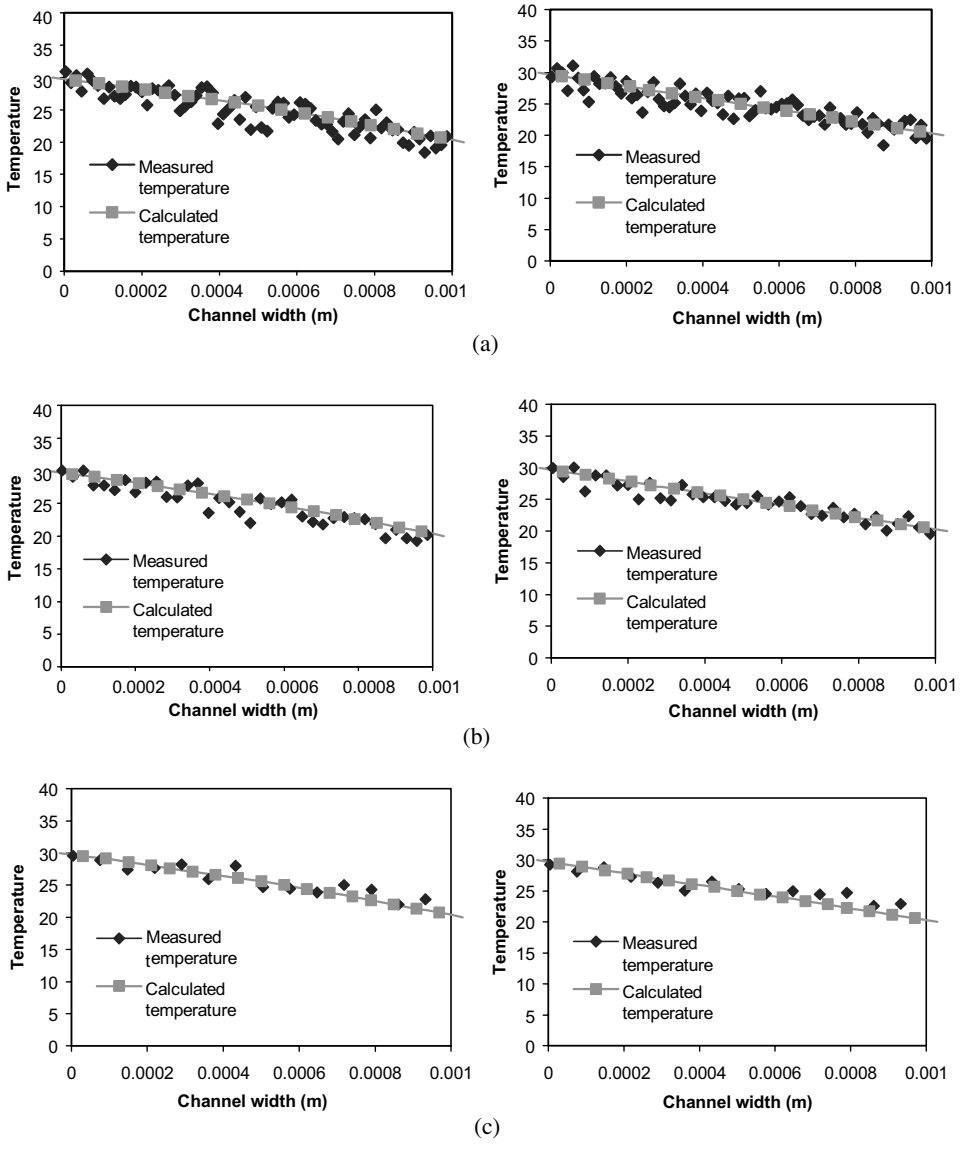

Fig. 5. Temperature profiles for the case of $Gr_wPr = 215$ ($T_L = 20$ °C and $T_H = 30$ °C): (a) spatial resolution: 19 μm (H) by 19 μm (V), (b) spatial resolution: 38 μm (H) by 38 μm (V), (c) spatial resolution: 76 μm (H) by 76 μm (V).

Table 2
Root-mean-square (r.m.s.) fluctuations of the measured temperature data from the predicted values for different spatial resolutions (Ref. to Fig. 5: $Gr_wPr = 215$; $T_L = 20$ °C and $T_H = 30$ °C)

Spatial resolution (μm × μm)	0.15 mm below the top	0.85 mm below the top
19 × 19	2.377 °C	2.306 °C
38 × 38	1.574 °C	1.566 °C
76 × 76	0.999 °C	0.924 °C

show fairly good agreement each other in that the temperature contours gradually deviate from the vertically stratified distributions with increasing Gr_wPr.

At such low Grashof–Prandtl numbers, there exists little free-convection current and the heat transfer occurs mainly by conduction across the fluid layer [25]. The horizontal variation in temperature should remain largely linear when the flow remains in the conduction regime of $Gr_wPr < 10^3$ as long as $h/w > 10$. Fig. 5 shows local and more quantitative comparisons between the measured and calculated temperature profiles at 0.15 mm (the left column), and 0.85 mm (the right column) below the top, for a representative case of $Gr_wPr = 215$. To examine the measurement uncertainties as a function of the spatial measurement resolution, the original pixel-by-pixel data are combined to 4×4, 8×8, and 16×16-pixeled interrogation cells, corresponding to the spatial resolution of 19 μm (H) by 19 μm (V), 38 μm by 38 μm, and 76 μm by 76 μm, respectively. Note that the spatial resolution for numerical calculations is remained as 58.8 μm (H) by 83.3 μm (V) for all the cases.

The data fluctuations should decrease with increasing number of the spatial samplings and the uncertainties are proportional to $1/\sqrt{N}$, for the case of multiple (N) samplings with N approaching to infinity. The root-mean-square (r.m.s.) fluctuations of the measured temperature data, from the calculated predictions, show persistent reduction from over 2 °C to below 1 °C, with measurement resolution changing from 19 μm square to 76 μm square (Table 2).

5. Conclusive remarks

A ratiometric (two-color) LIF technique has been examined primarily for its measurement uncertainties depending on the spatial resolution in order to explore the use for microscale full-field temperature mapping:

(1) The standard deviation of the temperature calibration, with 95% confidence level, range from ±1.967 °C for the 150 μm × 100 μm calibration field-of-view size, to 0.412 °C for 1200 × 800 μm view.
(2) For the tested 1.0-mm heated closed cuevette, the r.m.s. fluctuations of the measured temperature from the computational predictions show persistent decrease from 2.3 °C for 19 μm spatial measurement resolution to 0.92 °C for 76 μm resolution.

Acknowledgements

This material is based on the work supported by the National Center for Microgravity Research (NCMR). Dr. H.J. Kim wishes his gratitude for partial support arranged by Prof. J.S. Yoo of the National Research Laboratory (NRL) Program of Ajou University, established by the Ministry of Science and Technology, Korea. Any opinions, findings, and conclusions or recommendations expressed in this publication are those of the authors and do not necessarily reflect the view of the NCMR or the NRL.

References

[1] E.R.G. Eckert, R.J. Goldstein, Measurements in Heat Transfer, McGraw-Hill, New York, 1970.
[2] D. Dabiri, M. Gharib, Digital particle image thermometry and its application to a heated vortex ring, in: Fluid Measurement and Instrumentation Forum, ASME FED-95, 1990, pp. 27–34.
[3] D. Dabiri, M. Gharib, Digital particle image thermometry: the method and implementation, Exp. Fluids 11 (1991) 77–86.
[4] C.D. Richards, R.F. Richards, Transient temperature measurements in a convectively cooled droplet, Exp. Fluids 25 (1998) 392–400.
[5] M. Pehl, F. Werner, F.A. Delgado, First visualization of temperature fields in liquids at high pressure using thermochromic liquid crystals, Exp. Fluids 29 (2000) 302–304.
[6] D.R. Sabatino, T.J. Praisner, C.R. Smith, A high-accuracy calibration technique for thermochromic liquid crystal temperature measurements, Exp. Fluids 28 (2000) 497–505.
[7] J. Sakakibara, K. Hishida, M. Maeda, Vortex structure and heat transfer in the stagnation region of an impinging plane jet (simultaneous measurements of velocity and temperature fields by digital particle image velocimetry and laser-induced fluorescence), Int. J. Heat Mass Transfer 40 (13) (1997) 3163–3176.
[8] S.S. Chu, C.P. Grigoropoulos, Determination of kinetic energy distribution in a laser-ablated titanium plume by emission and laser-induced fluorescence spectroscopy, J. Heat Transfer 122 (2000) 771–775.
[9] T. Nakajima, M. Utsunomiya, Y. Ikeda, R. Matsumoto, Simultaneous measurement of velocity and temperature of water using LDV and fluorescence technique, in: The 5th Int. Symp. on Application of Laser Techniques To Fluid Mechanics, Lisbon, 1990, pp. 2.6.1–2.6.6.
[10] K. Sato, N. Kasai, Combined velocity and scalar field measurement with the simultaneous use of scanning PIV and LIF, in: The 10th Int. Symposium on Transport

Phenomena in Thermal Science and Process Engineering (ISTP10), 1997.
[11] M.C.J. Coolen, R.N. Kieft, C.C.M. Rindt, A.A. van Steenhoven, Application of 2-D LIF temperature measurements in water using a Nd-Yag laser, Exp. Fluids 27 (1999) 420–426.
[12] D.L. Andrews, Lasers in Chemistry, Springer-Verlag, Berlin, 1986.
[13] J. Coppeta, C. Rogers, Dual emission laser induced fluorescence for direct planar scalar behavior measurements, Exp. Fluids 25 (1998) 1–15.
[14] J. Sakakibara, R.J. Adrian, Measurement of whole field temperature using two-color LIF, J. Visual. Soc. Jpn. 17 (1997) 333–336.
[15] J. Sakakibara, R.J. Adrian, Whole field measurement of temperature in water using two-color laser induced fluorescence, Exp. Fluids 26 (1999) 7–15.
[16] S. Soloff, R.J. Adrian, Z. Liu, Distortion compensation for generalized stereoscopic particle image velocimetry, Meas. Sci. Technol. 8 (1997) 1441–1454.
[17] E. Hecht, Optics, fourth ed., Addison Wesley, Reading, 2002.
[18] J.R. Salor, Photobleaching of disodium fluorescein in water, Exp. Fluids 18 (1995) 445–447.
[19] American Association of Textile Chemists and Colorists, Color Index, 3rd ed., vol. 4, The Society of Dyers and Colorists, 1971.
[20] H.S. Choi, personal communications, Department of Chemical Engineering, Kyungil University, Kyungsan, Korea, 2003.
[21] A. Einstein, On the Movement of Small Particles Suspended in a Stationary Liquid Demanded by the Molecular-Kinetic Theory of Heat: Theory of the Brownian Movement, Dover Publications, New York, 1905, pp. 1–8.
[22] S.K. Friedlander, Smoke, Dust and Haze, Wiley, New York, 1977.
[23] A. Chuichi, Computational Fluid Dynamics for Engineering, University of Tokyo Press, Tokyo, 1994.
[24] S.V. Patankar, Numerical Heat Transfer and Fluid Flow, Taylor & Francis, New York, 1980.
[25] R.K. McGregor, A.P. Emery, Free convection through vertical plane layers: moderate and high Prandtl number fluids, J. Heat Transfer 91 (1969) 391–396.